Non-proportional mixed mode plasticity, crack tip fields from digital image correlation

S. Pommier, P.Y. Decreuse

LMT, École Normale Supérieure de Cachan, Cachan (France)
pommier@lmt.ens-cachan.fr

ABSTRACT. This paper is devoted to the experimental analysis of I+II mixed mode plasticity at crack tip using digital images correlation. The method employed to post-treat the experimental velocity fields is the same as that used in previous papers to post-treat finite element computations. The experimental velocity field is first partitioned into mode I and mode II components using symmetry considerations with respect to a coordinate system attached to the crack tip. Each mode is then partitioned into elastic and plastic parts. Each part is finally expressed as the product of an intensity factor and of a shape function, constructed once for all for a given material. With this approach, the experimental crack tip velocity field is fully characterized by four degrees of freedom $\left(\dot{\tilde{K}}_I, \dot{\rho}_I, \dot{\tilde{K}}_{II}, \dot{\rho}_{II}\right)$, which are respectively the intensity factors of the elastic and plastic part for each mode. The experimental results showed that the error associated with this approximation remains small. The error is also used for the determination of the yield surface of the crack tip region. The results show that the elastic domain of the crack tip region can be displaced in a $\left(K_I^\infty, K_{II}^\infty\right)$ space according to the plastic history experienced by the crack tip region. In addition, complex and non-intuitive evolutions of mixed mode plasticity were measured and explained with respect to the plastic history.

KEYWORDS. Mixed mode; Non-proportional; Plasticity; Yield threshold detection; Digital image correlation.

INTRODUCTION

A novel approach [1 - 3] was proposed to model the elastic-plastic behaviour of the crack tip region in a condensed manner for non-proportional mixed-mode loading conditions. The main assumption required by this approach is that the plastic zone is well confined inside an elastic medium. This has two main consequences :

- first, the loadings can be characterized by the nominal applied stress intensity factors $\left(K_I^\infty, K_{II}^\infty\right)$,
- second, the movement of the crack tip region is highly constrained and has thus a very limited number of degrees freedom.

The Karhunen-Loeve transform [4], which is based on the self-correlation matrix of the movement, is used to construct a basis of independent movements to which are associated independent degrees of freedom (intensity factors). We retain only the minimum number of degrees of freedom required to represent the crack tip velocity field with a sufficient precision. In addition, immediately after a load reversal, the behaviour of the crack tip region is transiently linear elastic and the approach should then coincide with the LEFM solutions. For this reason, the basis of independent movements contains at minimum the solutions obtained either for a mode I or a mode II linear-elastic loading phase. This approach was used in previous publications to post-treat finite element computations and it was shown that 4 degrees of freedom

(an "elastic" and a "plastic" one for each mode) are sufficient to represent the velocity field within the crack tip region with a very good accuracy. The velocity field is hence approximated as follows:

$$\underline{v}(P,t)_{R_0} = \left(\underline{v}(T,t)_{R_0} + \omega(R_T/R_0) \wedge \underline{TP}\right) + \underline{v}(P,t)_{R_T} \quad (1)$$

$$\underline{v}(P,t)_{R_T} \approx \underline{\tilde{v}}(P,t) = \underline{\tilde{v}}_e(P,t) + \underline{\tilde{v}}_{in}(P,t) \quad (2)$$

$$\underline{\tilde{v}}_e(P,t) = \dot{\tilde{K}}_I(t)\underline{u}_e^I(P) + \dot{\tilde{K}}_{II}(t)\underline{u}_e^{II}(P) \text{ and } \underline{\tilde{v}}_{in}(P,t) = \dot{\rho}_I(t)\underline{u}_c^I(P) + \dot{\rho}_{II}(t)\underline{u}_c^{II}(P) \quad (3)$$

In Eq. (1), the terms into brackets stem from the motion with respect to the reference frame R_O of the local frame R_T attached to the local crack plane and front T. This term is not the object of this analysis. It refers to the crack growth and deviation rate. The second term $\underline{v}(P,t)_{R_T}$ represent the velocity field for a fixed crack geometry. This term is approximated by the sum $\underline{\tilde{v}}(P,t)$ of an elastic part $\underline{\tilde{v}}_e(P,t)$ and a plastic part $\underline{\tilde{v}}_{in}(P,t)$. The mode I and mode II components of each of them correspond respectively to their symmetric and anti-symmetric parts with respect to the local crack plane and tip. The shape functions $\left(\underline{u}_e^I, \underline{u}_e^{II}, \underline{u}_c^I, \underline{u}_c^{II}\right)$ are constructed a priori for a given material, their intensity factors $\left(\dot{\tilde{K}}_I, \dot{\tilde{K}}_{II}, \dot{\rho}_I, \dot{\rho}_{II}\right)$ are the independent degrees of freedom of the problem. With this hypothesis, $\left(\dot{\rho}_I, \dot{\rho}_{II}\right)$ is a condensed measure of crack tip plasticity in mixed mode conditions. To check the validity of this approach, the error associated with the approximation in Eq. (2) and (3) is also determined at each time step. In practice, it is useful to define two errors :

- the error $C_{1R}(t)$, associated with an elastic representation of the velocity field
- the error $C_{2R}(t)$, associated with an elastic-plastic representation of the velocity field.

$$C_{1R}(t) = \sqrt{\frac{\int_{P\in D}\left(\underline{v}(P,t)_{R_T} - \underline{\tilde{v}}_e(P,t)\right)^2 dP}{\int_{P\in D}\left(\underline{v}(P,t)_{R_T}\right)^2 dP}}, \quad C_{2R}(t) = \sqrt{\frac{\int_{P\in D}\left(\underline{v}(P,t)_{R_T} - \underline{\tilde{v}}_e(P,t) - \underline{\tilde{v}}_{in}(P,t)\right)^2 dP}{\int_{P\in D}\left(\underline{v}(P,t)_{R_T}\right)^2 dP}} \quad (4)$$

In the following, the criterion $C_{1R}(t)$-$C_{2R}(t)$<y%, is used as a yield criterion. As a matter of fact, if the elastic-plastic approximation of the computed or measured displacement field is not better than the elastic one, enriching the elastic approximation to account for plasticity is useless. The crack tip region can therefore be considered as behaving essentially elastically. This criterion was hence used to post-treat finite element computation and allowed visualizing yield surfaces in mixed mode conditions, which matched very well the theoretical yield criterion [2, 3] for the crack tip region (elastic distortional energy criterion [8]).

EXPERIMENTS

Experimental setup

The tri-axial testing machine ASTREE, available at LMT-Cachan, is used for this experiment. Its 4 horizontal actuators are used. They have a load capacity of 100 kN and a 250 mm stroke range and can be freely and independently relocated along the vertical columns of the frame. For this test, they are placed in the same horizontal plane. A special control mode is used to « balance » the load between the two actuators of each axis, so as to keep the centre of the specimen motionless.

A cruciform specimen (Fig. 1 a) was machined in a S355 NL ferritic-pearlitic steel used in marine applications. A thin slit was made by electro-erosion at the centre of the specimen with a plane inclined at an angle of 45° towards the axes of the specimen. The crack remained co-planar during mode I pre-cracking until it reached a size 2a=30mm.

A preliminary elastic analysis of the problem by the FEM allowed to determine the relations between the loads (F_x,F_y) applied by the actuators and the nominal stress intensity factors $\left(K_I^\infty, K_{II}^\infty\right)$. A pure mode I condition is obtained if F_x=F_y and a pure mode II if F_x=-F_y.

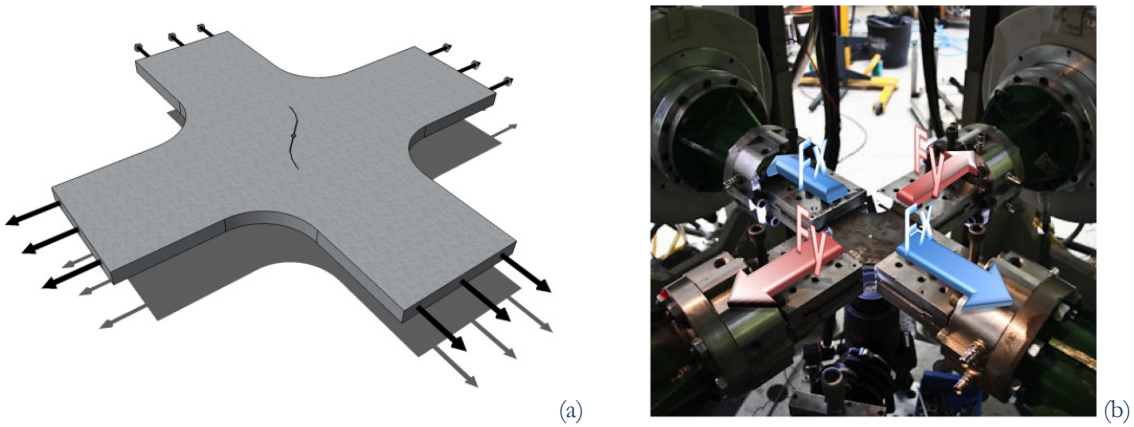

(a) (b)

Figure 1: (a) cruciform specimen used in the experiments, (b) the triaxial testing machine ASTREE. In this machine the centre of the specimen can be kept motionless.

A digital single lens reflex camera (Canon EOS 5D) was placed under the specimen and triggered by the load controller, so as to associate each image to a point in the loading sequence. The used prime lens (Canon MP-E 65mm f/2.8 Macro) enabled acquiring images whose corresponding sizes on the sample were as small as 3 mm x 3 mm, so that each pixel size was 2.9 μm x 2.9 μm. The images were post-treated to determine the velocity field using a digital images correlation (DIC) technique. The used approach was global, based on a continuous description of the displacement field over a finite-element mesh [7]. In the present case the mesh was composed of regular triangles, and the displacement was bilinear on each element. The whole procedure was performed using the LMTpp programming plateform of the LMT Cachan laboratory. As for any other DIC technique [5 - 7], the measurement uncertainty is strongly dependent on the quality of the speckle covering the specimen. This uncertainty was determined by numerically applying a known rigid body motion to the specimen and by comparing the displacement field measured using the DIC technique with the applied one. The speckle, sprayed by a fine airbrush, was optimized so as to finally get an uncertainty equal to 0.07 μm on the measured displacement field with 32 pixel-sided triangles.

Digital image correlation and post-treatments of DIC fields

Each image is compared to the previous one in the loading sequence in order to measure the displacement field in each time step at the surface of the specimen. First of all, the crack tip and the crack plane are roughly determined from DIC measurements, using the normalised correlation error. As a matter of fact, the algorithm used to analyse digital images assumes that the displacement field is piecewise linear within 32 pixel-sided triangles. Along the crack plane, the displacement field is discontinuous and hence very far from being piecewise linear, therefore the correlation error can be used to find the crack plane and the crack tip. Once the crack plane is located, the region of the image located in its vicinity is excluded from the analysis using a mask, so as to minimize the measurement errors. The images are then cropped to position the tip of the crack in the centre and the crack plane midway. This operation is equivalent to remove the rigid body motion from the total displacement field between two time steps. Then the displacement field $\underline{d\tilde{u}}(P,t)$ relative to the frame attached to the crack plane and tip, is extracted from the sequence of images. Finally, it is partitioned into mode I and mode II components as follows:

$$\underline{d\tilde{u}}(P,t) = \underline{d\tilde{u}}(x,y,t) = \underline{d\tilde{u}}_I(x,y,t) + \underline{d\tilde{u}}_{II}(x,y,t) \tag{5}$$

with:

$$\begin{cases} 2du_I^x(x,y,t) = du_I^x(x,y,t) + du_I^x(x,-y,t) \\ 2du_I^y(x,y,t) = du_I^y(x,y,t) - du_I^y(x,-y,t) \end{cases} \text{ and } \begin{cases} 2du_{II}^x(x,y,t) = du_{II}^x(x,y,t) - du_{II}^x(x,-y,t) \\ 2du_{II}^y(x,y,t) = du_{II}^y(x,y,t) + du_{II}^y(x,-y,t) \end{cases} \tag{6}$$

Construction of the shape functions $\left(u_e^I, u_e^{II}, u_c^I, u_c^{II}\right)$

The crack is cyclically loaded in mode I at a positive stress ratio to avoid crack closure. Then a mode I cycle is applied for which images are recorded at the peak load, and below the peak load for the same load level before the peak and after unloading from the peak. For instance :

- at t_1, $K_I^\infty = 21MPa\sqrt{m}$
- at t_2, $K_I^\infty = 25MPa\sqrt{m}$
- at t_3, $K_I^\infty = 21MPa\sqrt{m}$

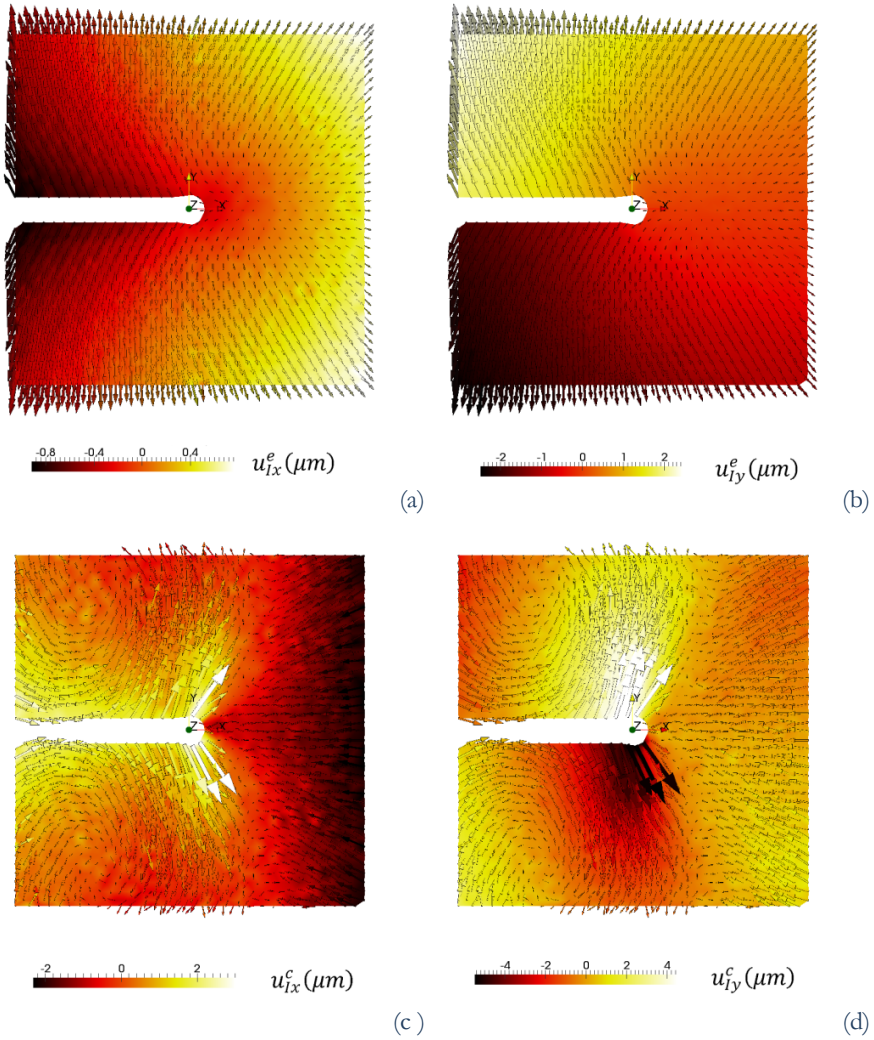

Figure 2: Mode I shape functions constructed using DIC. (a) component $u_c^I{}_x$ of the elastic field, (b) component $u_c^I{}_y$ of the elastic field, (c) component $u_c^I{}_x$ of the plastic field, (d) component $u_c^I{}_y$ of the plastic field.

The unloading phase (between t_2 and t_3) is considered as essentially elastic, because $\Delta K_I^\infty < \Delta K_I^{th}$. It is used to construct the mode I elastic reference field, which is defined as being equal to the mode I part of the displacement field between t_3 and t_2 non-dimensioned by $K_I^\infty = 4MPa\sqrt{m}$.

$$\underline{u}_e^I(P) = \frac{\underline{u}_{DIC}^I(P, t_2 \to t_3)}{4MPa\sqrt{m}} \tag{7}$$

It is also checked that the mode II part of the displacement field is negligible. Then, the displacement field between t_1 and t_3 is recorded. Since the nominal applied stress intensity factor is the same in both cases, the elastic part of the displacement field is not dominant. However, though the nominal applied stress intensity factor is the same in t_1 and t_2, the displacement field between t_1 and t_3 is not entirely plastic. As a matter of fact, since the plastic zone is confined, crack tip plasticity is associated with the development of internal stresses. Their contribution to the crack tip velocity field is similar to that of the macroscopic stresses. It has to be removed from the displacement recorded between t_1 and t_3 to

construct the plastic field (Eq. 8). The residue is non-dimensioned by the average β of its discontinuity across the crack faces so that the intensity factor ρ_I could also be read as the CTOD, which makes possible using the Li's criterion [9] as a crack growth criterion.

$$\underline{u}_c^I(P) = \beta^{-1}\left(\underline{u}_{DIC}^I\left(P, t_1 \to t_3\right) - \Delta\tilde{K}_I^{t_1 \to t_3}\underline{u}_e^I(P)\right) \tag{8}$$

$$\Delta\tilde{K}_I^{t_1 \to t_3} = \frac{\sum_P \underline{u}_{DIC}^I\left(P, t_1 \to t_3\right).u_e^I(P)}{\sum_P u_e^I(P).u_e^I(P)} \tag{9}$$

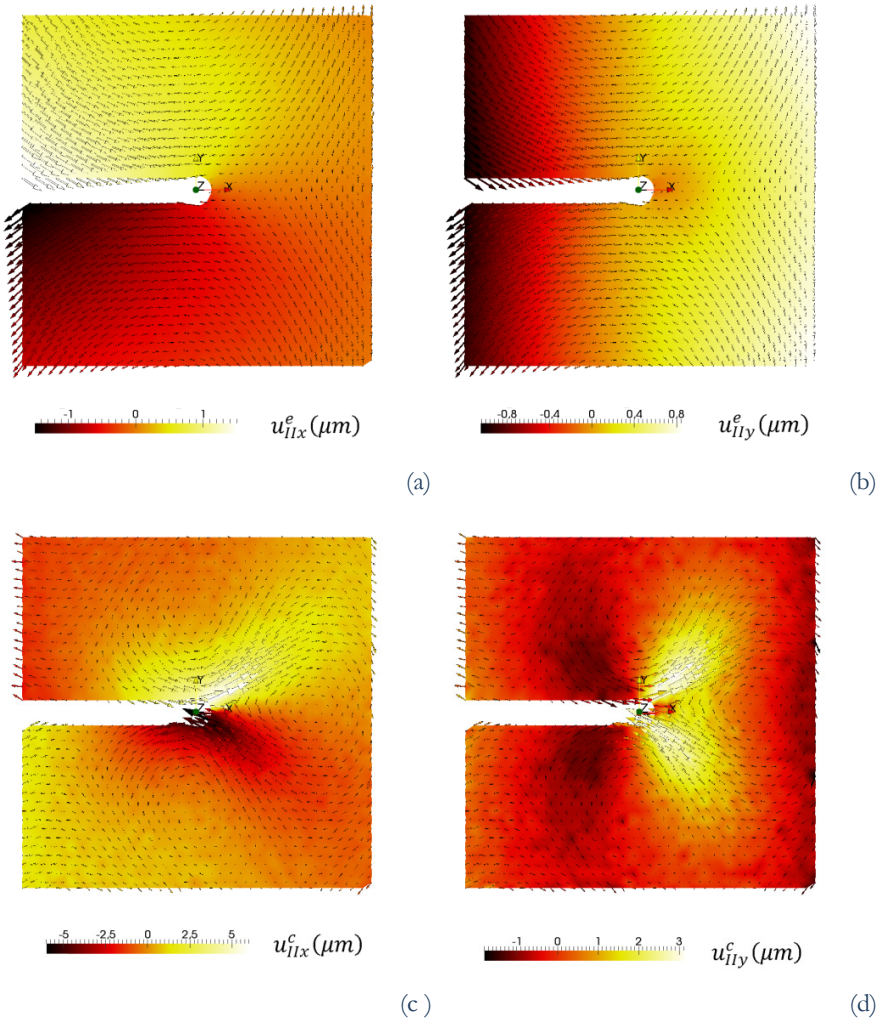

Figure 3: Mode II shape functions constructed using DIC. (a) component $u_e^{II}{}_x$ of the elastic field, (b) component $u_e^{II}{}_y$ of the elastic field, (c) component $u_c^{II}{}_x$ of the plastic field, (d) component $u_c^{II}{}_y$ of the plastic field.

The same approach is used to construct the mode II elastic and plastic shape functions. The two components of the four shape functions $\left(u_e^I, u_e^{II}, u_c^I, u_c^{II}\right)$ are plotted in Fig. 2 and Fig. 3. The elastic fields are qualitatively similar to the Westergaard solutions. However, the analytical solution is not used, because it corresponds to an ideal 2D problem, while, in the experiment, we don't know the inclination of the crack plane and front with respect to the specimen surface. In addition, the Westergaard's analytical solution is an asymptotic solution, while we aim at analysing a 1mm sided domain.

RESULTS

Extraction and evolution of the intensity factors

Once the shape functions are determined, using the preliminary experiments described above, they can be used to post-treat the displacement fields measured during complex sequences, provided that the growth of the crack remains small (well below 100 μm).

During a mixed mode load increment $\left(dK_I^\infty, dK_{II}^\infty\right)$ the crack tip displacement field $d\underline{u}_{DIC}(P,dt)$ is determined at each time step. The variations of the four intensity factors during the step are ^determined as follows:

$$d\tilde{K}_{I\ or\ II} = \frac{\sum_P \underline{u}_{DIC}(P,dt).u_e^{I\ or\ II}(P)}{\sum_P u_e^{I\ or\ II}(P).u_e^{I\ or\ II}(P)} \quad d\rho_{I\ or\ II} = \frac{\sum_P \underline{u}_{DIC}(P,dt).u_c^{I\ or\ II}(P)}{\sum_P u_c^{I\ or\ II}(P).u_c^{I\ or\ II}(P)} \tag{10}$$

An example of such a measurement is plotted in Fig. 4. The mode II plastic intensity factor $\rho_{II} = \int d\rho_{II}$ is plotted versus the Mode II nominal applied stress intensity factor. The evolutions measured using Digital images correlation are qualitatively consistent with the results of finite element simulations [2, 3]. During a loading sequence, there are phases during which $d\rho_{II}$ is very small, that can be considered as an elastic domain for the crack tip region.

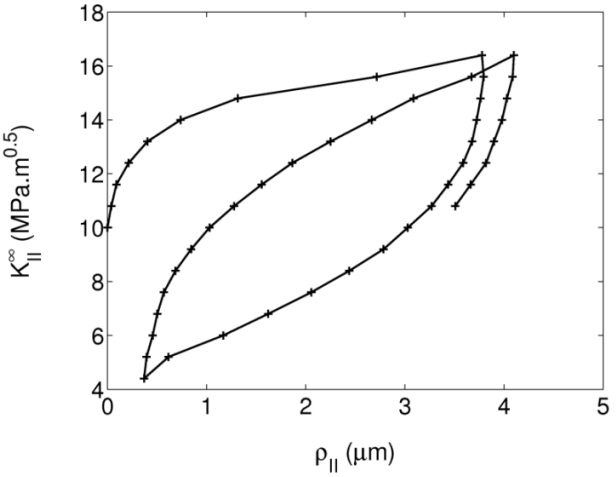

Figure 4: Evolution of the condensed measure ρ_{II} of Mode II plasticity as a function of the mode II nominal applied stress intensity factor K_{II}^∞. Measurement performed using digital image correlation (DIC), during a mode II loading phase ΔK_{II}^∞=12MPa√m around a mean value (K_{II}^∞=30MPa√m, K_{II}^∞=0).

Yield surface and the elastic domain

As it was discussed in the introduction, the criterion $C_{1R}(t)$-$C_{2R}(t)$<y% can be used as a yield criterion. The crack tip region is considered as behaving essentially elastically if the elastic-plastic approximation of the measured displacement field is not better than the elastic one.

The following procedure was hence applied to construct the elastic domain experimentally. First of all, the structure is loaded to a given centre point $\left(\overline{K}_I^\infty, \overline{K}_{II}^\infty\right)$. Then loading cycles, with a mean value $\left(\overline{K}_I^\infty, \overline{K}_{II}^\infty\right)$ and a decreasing amplitude, are applied so as to stabilize the elastic domain around the centre point. Then, from this point, radial loading directions are explored sequentially. For each direction, two loading cycles are applied, the criterion C_{1R}-C_{2R} is extracted from the first cycle and plotted in a $\left(K_I^\infty, K_{II}^\infty\right)$ diagram as a colour level. 15 cycles with cyclically decreasing amplitude are then applied along the current explored direction to re-stabilize the elastic domain. A new direction is later explored. The results are plotted in Fig. 5 (a).

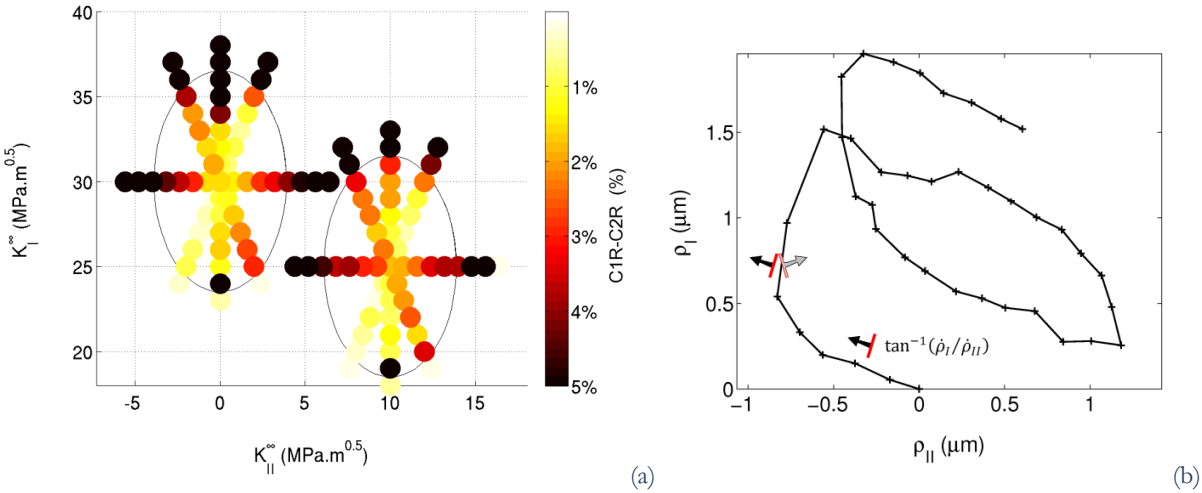

Figure 5: (a) Experimental construction of the elastic domain of the crack tip region. C_{1R}-C_{2R} is determined in each time increment, and plotted in a $\left(K_I^\infty, K_{II}^\infty\right)$ diagram as a colour level for each increment. High values of the criterion are darker and indicate a high plasticity rate. (b) Experimental plastic flow direction measured during two radial mixed mode loading cycle with around the central point $\left(\overline{K}_I^\infty = 30MPa\sqrt{m}, \overline{K}_{II}^\infty = 0\right)$.

The procedure was automated, so as to construct the elastic domain for two different locations of the central point. In this figure, it can be observed that the C_{1R}-C_{2R} displays its minimum values roughly around the central point. If the distance to the central point increases, C_{1R}-C_{2R} increases whatever the loading direction that is explored. This result is consistent with the generalized von Mises criterion of the model [3], which is an ellipse in a $\left(K_I^\infty, K_{II}^\infty\right)$ diagram. In the experiments, the dimension of the elastic domain is found to be larger along a mode I loading direction than along a mode II one, which is also consistent with the model. In Fig. 5 (a), the plotted ellipses do have a shape factor of 1.65 and their size is adjusted to fit C_{1R}-C_{2R}=4% . In addition, these experimental results show clearly that the elastic domain can be displaced accord to the plastic history viewed by the crack tip region. This is consistent with the choices that were done to model crack tip plasticity, i.e. introducing an internal stress intensity factor $\left(K_I^X, K_{II}^X\right)$ analogous to a kinematic hardening term that stands for internal stresses stored at crack tip.

Plastic flow direction

For each radial loading direction explored around the central point, it is also possible to determine the plastic flow direction at each time step. It was found in the experiments that the plastic flow directions could remain exactly the same during quite a few steps and then change quite drastically though the loading direction remains the same (Fig. 5 (b)).

As a matter of fact, since the rate $\dot{a}$ of creation of cracked area per unit length of crack front is assumed to be proportional to the plasticity rate $\dot{\rho}$, consistently with the Li's criterion [9] the thermodynamic force associated with $\dot{\rho}$ should be homogeneous to that associated with $\dot{a}$, this is to say G. For this reason, two forces G_I and G_{II}, associated respectively with $\dot{\rho}_I$ and $\dot{\rho}_{II}$ were introduced [2,3] with $G_{I\,or\,II} = sign\left(K_{I\,or\,II}^\infty - K_{I\,or\,II}^X\right)\left(K_{I\,or\,II}^\infty - K_{I\,or\,II}^X\right)^2 / E^*$. Plotted in a $\left(G_I, G_{II}\right)$ diagram, the generalized von Mises criterion [8] used in the model has now a diamond shape. At the summits of this diamond, a normality flow rule implies that the flow direction changes very significantly for a very small change in the loading direction. Along the faces of the diamond, the flow direction is constant which is what we observe in the experiments (Fig. 5 b).

CONCLUSIONS

This paper was devoted to the experimental analysis of non-proportional mixed mode plastic deformation within the crack tip region, so as to validate a novel approach to model the mixed mode elastic-plastic behaviour of a cracked component on a global scale.

The velocity field at the vicinity of the crack tip was determined using digital image correlation in I+II mixed mode loading conditions. The mode I and mode II components of the experimental velocity field were extracted using symmetry considerations with respect to a coordinate system attached to the crack tip.
Each mode was then partitioned into elastic and plastic parts and each part was approached by the product of an intensity factor and a shape function, constructed once for all. With this approach, the experimental velocity field is described using four degrees of freedom only, $\left(\dot{\tilde{K}}_I, \dot{\rho}_I, \dot{\tilde{K}}_{II}, \dot{\rho}_{II}\right)$ which are respectively the mode I and mode II intensity factors of the elastic and plastic part of the velocity field. The experimental results showed that the error associated with this approximation is small.
A criterion based on the errors was proposed to determine the yield surface, and it was shown that the experimental yield surface is consistent with the theoretical one. In particular it is shown experimentally that the crack tip region displays an elastic domain which centre can move according to the plastic history. This elastic domain is closed by a yield surface, plasticity may occur either in tension or in compression.
The plastic flow direction was also determined using digital image correlations. There are phases for which that flow direction is constant and sudden changes of the flow direction for a constant loading direction are also observed. This results is consistent with the diamond shape elastic domain used in the model.

ACKNOWLEDGEMENTS

This work is supported by the French National Research Agency (ANR) through the project MIXMODFATFIS (No. BLAN06-1_134492) and by the Research Agency of the French Ministry of Defence (DGA).

REFERENCES

[1] S. Pommier, R. Hamam, Fatigue Fract. Engng Mater. Struct., 30 (7) (2007) 582.
[2] R. Hamam, S. Pommier, F. Bumbieler, Int. J. of Fatigue, 29 (9-11) (2007) 1634.
[3] S. Pommier, P. Lopez-Crespo, P. Y. Decreuse, Fatigue Fract Eng Mater Struct, 32 (2009) 899.
[4] K. Karhunen, Mat.-Phys., 37 (1947) 1.
[5] T. C. Chu, W. F. Ranson, M. A. Sutton, W. H. Peters, Experimental Mechanics, 25 (1985) 232.
[6] H. A. Bruck, S. R. McNeill, M. A. Sutton, W.H. Peters, Experimental Mechanics, 29 (1989) 261.
[7] G. Besnard, F. Hild, S. Roux, Experimental Mechanics, 46 (6) (2006) 789.
[8] J. Qian, A. Fatemi, Engineering Fracture Mechanics, 55 (6) (1996) 969.
[9] C. Li, Fatigue Fracture Engng Mater.Structures, 12 (1989) 59.